Intercomparison of Unmanned Aircraftborne and Mobile Mesonet Atmospheric Sensors

ADAM L. HOUSTON

Department of Earth and Atmospheric Sciences, University of Nebraska–Lincoln, Nebraska

ROGER J. LAURENCE III AND TEVIS W. NICHOLS

Department of Aerospace Engineering Sciences, University of Colorado Boulder, Boulder, Colorado

SEAN WAUGH

Cooperative Institute for Mesoscale Meteorological Studies, University of Oklahoma, and National Oceanic and Atmospheric Administration/National Severe Storms Laboratory, Norman, Oklahoma

BRIAN ARGROW

Department of Aerospace Engineering Sciences, University of Colorado Boulder, Boulder, Colorado

CONRAD L. ZIEGLER

National Oceanic and Atmospheric Administration/National Severe Storms Laboratory, Norman, Oklahoma

(Manuscript received 1 September 2015, in final form 15 May 2016)

ABSTRACT

Results are presented from an intercomparison of temperature, humidity, and wind velocity sensors of the Tempest unmanned aircraft system (UAS) and the National Severe Storms Laboratory (NSSL) mobile mesonet (NSSL-MM). Contemporaneous evaluation of sensor performance was facilitated by mounting the Tempest wing with attached sensors to the NSSL-MM instrument rack such that the Tempest and NSSL-MM sensors could collect observations within a nearly identical airstream. This intercomparison was complemented by wind tunnel simulations designed to evaluate the impact of the mobile mesonet vehicle on the observed wind velocity.

The intercomparison revealed strong correspondence between the temperature and relative humidity (RH) data collected by the Tempest and the NSSL-MM with differences generally within sensor accuracies. Larger RH differences were noted in the presence of heavy precipitation; however, despite the exposure of the Tempest temperature and humidity sensor to the airstream, there was no evidence of wet bulbing within precipitation. Wind tunnel simulations revealed that the simulated winds at the location of the NSSL-MM wind monitor were ~4% larger than the expected winds due to the acceleration of the flow over the vehicle. Simulated vertical velocity exceeded 1 m s^{-1} for tunnel inlet speeds typical of a vehicle moving at highway speeds. However, the theoretical noncosine reduction in winds that should result from the impact of vertical velocity on the laterally mounted wind monitor was found to be negligible across the simulations. Comparison of the simulated and observed results indicates a close correspondence, provided the crosswind component of the flow is small.

1. Introduction

The Airdata Verification and Integrated Airborne Tempest Experiment (AVIATE), a collaboration involving the Research and Engineering Center for Unmanned

Corresponding author address: Dr. Adam L. Houston, Department of Earth and Atmospheric Sciences, University of Nebraska–Lincoln, 214 Bessey Hall, Lincoln, NE 68588.
E-mail: ahouston2@unl.edu

DOI: 10.1175/JTECH-D-15-0178.1

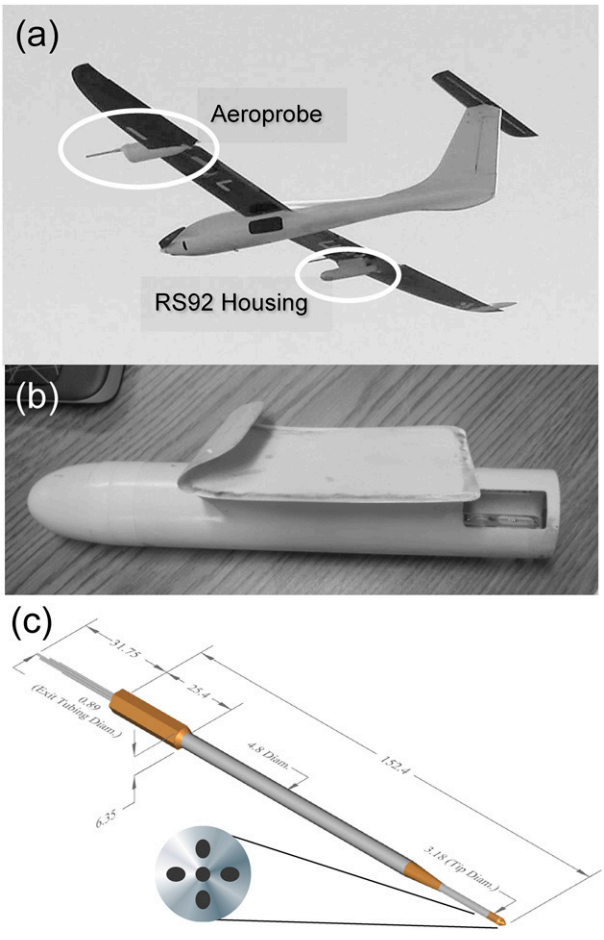

FIG. 1. (a) Tempest unmanned aircraft as configured for AVIATE. The placement of the temperature/moisture sensor (Vaisala RS92) and the wind velocity sensor (Aeroprobe five-port probe) is annotated. (b) Rocket nose and wing sleeve for the RS92 temperature/humidity sensor (the RS92 is visible at the rear of the rocket nose through one of three vents). (c) Aeroprobe five-port probe.

Vehicles at the University of Colorado Boulder, the University of Nebraska–Lincoln, and NOAA's National Severe Storms Laboratory (NSSL), was conducted in June 2013. The principal objective of AVIATE was to evaluate the temperature, humidity, and wind velocity sensors of the Tempest unmanned aircraft system (UAS; Fig. 1) and the NSSL mobile mesonet (MM; Fig. 2). The Tempest UAS (Elston et al. 2011; Frew et al. 2012) is a versatile, state-of-the-art system built on a legacy of successful applications of UAS sampling transient mesoscale phenomena (Elston et al. 2011; Frew et al. 2012; Houston et al. 2012). The aircraft is the product of a collaboration between the Research and Engineering Center for Unmanned Vehicles (RECUV) at the University of Colorado Boulder and UASUSA (www.uasusa.com). It has a high-aspect ratio wing with a span of 3.2 m and a maximum gross takeoff weight of 6.8 kg [the reader is referred to Elston et al. (2011) for more information on the Tempest]. The mobile mesonet is a mobile weather-observing system composed of a meteorological instrument package and a ground-based vehicle on which it is mounted. The NSSL-MM version used for AVIATE was initially employed in the 2010 field phase of the second Verification of the Origins of Rotation in Tornadoes Experiment (VORTEX2; Wurman et al. 2012).

The rapid proliferation of UAS applications to the atmospheric sciences [the reader is referred to the reviews of Houston et al. (2012) and Elston et al. (2015)] means that the results of sensor intercomparisons and the methodologies for conducting them are important to document. In contrast to UAS, MMs have a long track record of collecting in situ near-surface meteorological observations (e.g., Rasmussen et al. 1994; Straka et al. 1996; Markowski 2002; Lang et al. 2004; Weckwerth et al. 2004; Ziegler et al. 2007; Waugh and Frederickson 2010; Wurman et al. 2012). However, systematic evaluations of MM sensor performance are uncommon (e.g., Skinner et al. 2010; Waugh and Frederickson 2010).

The relevant sensors for the Tempest and NSSL-MM are listed in Table 1. The use of a radiosonde-type temperature/moisture sensor in the Tempest has precedent in the sensor suite of the Aerosonde (Holland et al. 2001), the University of Colorado (CU) NexSTAR (Houston et al. 2012), and the powersonde (Douglas 2008). The Vaisala RS92 used for this work has been adapted by the National Center for Atmospheric Research's Earth Observing Laboratory to reduce its form factor for use in the Miniature In-situ Sounding Technology (MIST) dropsonde. On the Tempest, the sensor is housed in a radiosonde tube, capped with a rocket nose cone and mounted under the wing (Figs. 1a and 1b). The underwing mount shields the sensor from direct sunlight and three side vents along with an open tail enable exposure to the airstream. These data are logged at 2 Hz.

The wind velocity sensor on the Tempest is the Aeroprobe Corp. five-port pitch+yaw probe model PSPY5-H794–254 (Fig. 1c). Aircraft sideslip and angle of attack can be deduced through differential pressure measured across the probe tip. Along with aircraft attitude and ground velocity (measured independently), the ground-relative (inertial) wind velocity can be deduced. These data are logged by a model On the Fly! Air Data System (OTF-ADS) air data computer that, by virtue of the short (~10 cm) hose length, has an output data rate of 100 Hz.

On the NSSL-MM, a shielded and aspirated system called the U-tube (Fig. 2) houses the HMP45C (humidity and slow temperature) and the YSI 405 (fast

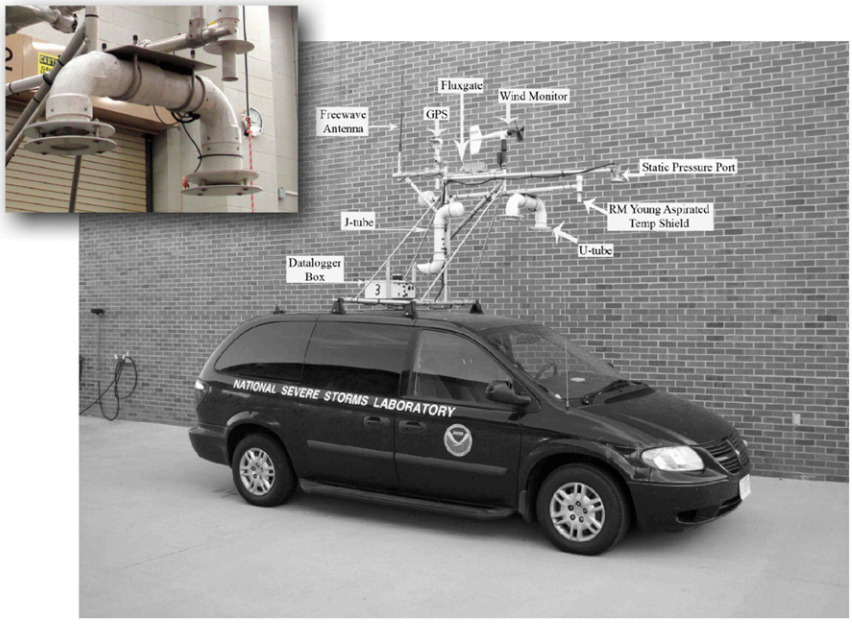

FIG. 2. NSSL-MM. The present study discusses observations from the R. M. Young "wind monitor," the R. M. Young fast-response "aspirated temperature" sensor, and the slow-response temperature and RH sensors housed in the "U-tube" (see also inset photo).

temperature) sensors (Waugh and Frederickson 2010; S. M. Waugh 2012, meeting presentation). The U-tube is mounted ~2.7 m above the ground. The R. M. Young wind monitor (propeller-vane anemometer) is mounted ~3.3 m above the ground and ~2.4 m rear of the leading edge of the vehicle. Using independently observed ground velocity, the ground-relative (inertial) wind velocity can be deduced. This ground-relative velocity is intended to represent the upstream wind field that is unmodified by the vehicle. These data are logged at 1 Hz.

While the individual sensors of the Tempest and the NSSL-MM have previously undergone extensive testing,

TABLE 1. List of relevant sensors and their characteristics for the Tempest and NSSL-MM.

Variable	Tempest	NSSL-MM
Temperature (fast response)	Vaisala RS92 core (MIST integration[a]) Accuracy: ±0.5 K[b] Response time: <0.4 s[c]	YSI 405 thermistor Accuracy: ±0.1 K Response: 10 s
Temperature (slow response)	—	Campbell Scientific HMP45C[d] ±2 K[e] Unspecified response time
Humidity	Vaisala RS92 core (MIST integration[a]) Accuracy: ±5%[b] Response time: <0.5 s[c]	Campbell Scientific HMP45C ±2% 15 s[f]
Wind	Aeroprobe Corp. five-port pitch+yaw probe ±0.1° flow angle error (for angles of ±20°)[g] ±0.06 m s^{-1} velocity error[g]	R. M. Young wind monitor (four-blade helicoid propeller and vane) ±3° flow angle error[h] ±0.3 m s^{-1} velocity error (or 1%)[h]

[a] http://www.eol.ucar.edu.
[b] Cumulative uncertainty; http://www.vaisala.com/.
[c] The *e*-fold response in 6 m s^{-1} flow and 1000 hPa; http://www.vaisala.com/.
[d] Manufactured by Vaisala Inc. but cabled and modified for logging by Campbell Scientific.
[e] At 20°C and RH < 90%; http://www.campbellsci.com/.
[f] The 90% response at 20°C; http://www.campbellsci.com/.
[g] For a 30 m s^{-1} relative flow velocity (Aeroprobe Corp. 2012).
[h] http://www.youngusa.com/products/7/5.html.

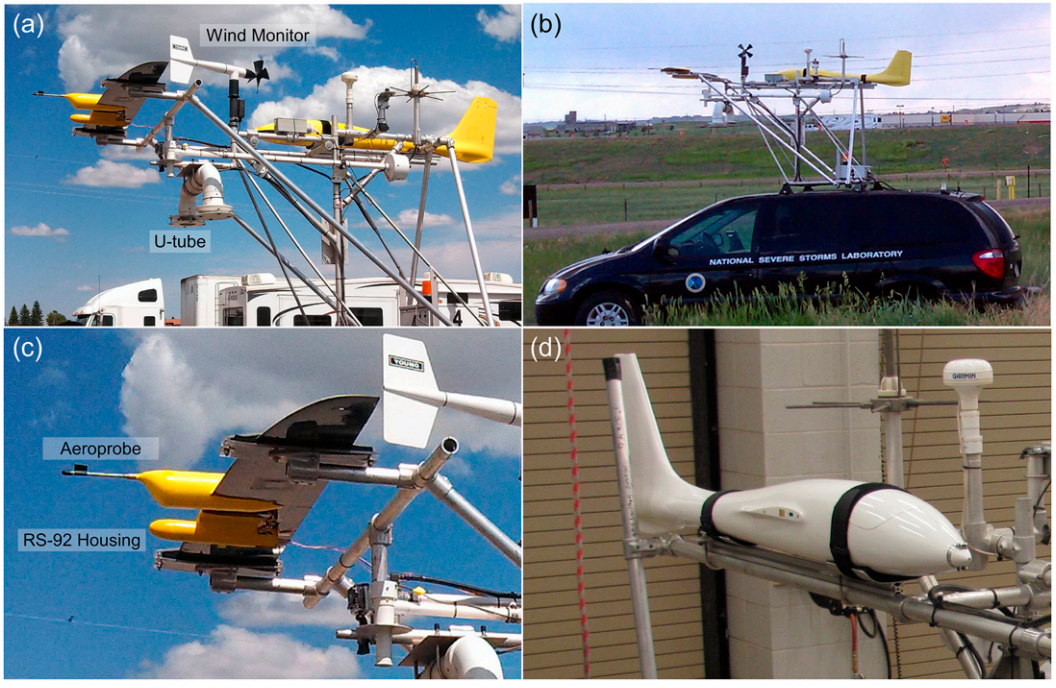

FIG. 3. (a) Integrated system via a specially augmented (b) rooftop rack assembly implemented by coauthor SW for AVIATE. Illustrated in (c) and (d) are the methods used to mount the wing with the Aeroprobe and RS-92 (temperature/humidity) sensors, and the fuselage to the MM rack, respectively.

and comprehensive performance metrics are available from the sensor manufacturers, the performance of these sensors when integrated into each platform remains to be evaluated. The following potential performance issues are the focus of the experiments presented herein:

- Exposure of the Tempest temperature/moisture sensor makes it susceptible to wetting in precipitation and erroneous wet bulbing.
- The U-tube housing for the temperature/moisture sensors of the NSSL-MM reduces the sensor response.
- The NSSL-MM vehicle will significantly modify the wind field above the vehicle, which could have a significant impact on the observed wind velocity.

The present article proceeds with a description of the experiment methodology adopted during AVIATE; followed by a presentation of the temperature, moisture, and wind velocity analyses in section 3; and a summary of the principal findings in section 4.

2. Methodology

While the experiment control afforded by conducting sensor comparisons in the laboratory is of great value, the objective of these experiments was to examine sensor performance in more realistic atmospheric conditions. However, without the ability to approximately replicate the environment for repeated experiments with each sensor, as in laboratory-based comparisons, it was essential that the sensor suites were nearly collocated. This collocation was enabled by mounting the Tempest wing to the NSSL-MM instrument rack (Fig. 3) such that the wing-mounted temperature/humidity and wind sensors could collect observations contemporaneous with the NSSL-MM sensors and within a nearly identical airstream at speeds similar to the typical airspeed of the Tempest (20–30 m s^{-1}). The fuselage was strapped onto a bracket designed to transport the aircraft and the bracket was bolted to the mesonet rack (Fig. 3). The wing was compressed between two foam-lined polycarbonate plates (Fig. 3). Although the collocated NSSL-MM and Tempest sensors (referred to as the integrated system) could be compared without the NSSL-MM vehicle (i.e., the entire rack could be placed in a wind tunnel), mounting both systems to the vehicle enabled the investigators 1) to examine sensor sensitivity in a variety of mesoscale atmospheric phenomena (i.e., these phenomena could be "chased") and 2) to examine the impact of the vehicle on the airstream within which both sensor suites resided. Moreover, by incorporating the wing along with the sensors, the potential effects of the wing on the sensors would be included in the observations.

To expose the Tempest temperature and humidity sensors to the potential biasing effects of wetting, the

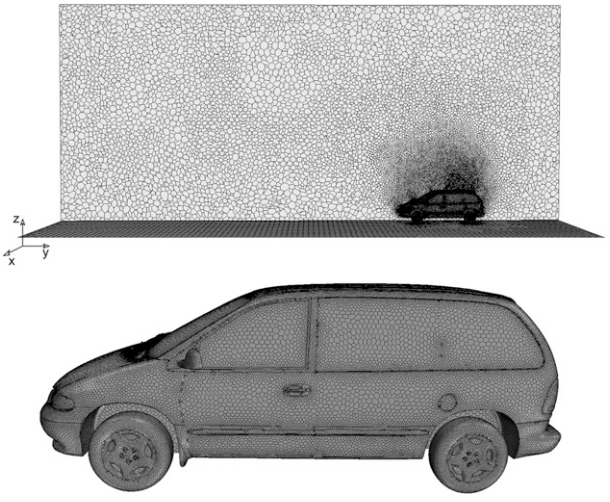

FIG. 4. Mesh for wind tunnel simulations.

integrated system was deployed into moderate–heavy precipitation. Sensor wetting should manifest as short periods of anomalously cold (approaching the wet-bulb temperature) and humid (approaching a relative humidity of 100%) observations, relative to the data from the (shielded) NSSL-MM sensors. To compare the temperature and humidity sensor responses, the integrated system was tasked to execute transects across airmass boundaries.

Both lateral and vertical accelerations of the mean-state (nonturbulent) flow produced by the NSSL-MM vehicle are to be expected. Since, the NSSL-MM wind monitor is intended only to measure the lateral component of the flow, the intercomparison will focus on the consistency between the observed lateral wind velocities. However, the vertical velocity can have a significant impact on the lateral wind speed measured by a propeller-vane anemometer (Drinkrow 1972). Since the Tempest anemometer is capable of decomposing the wind velocity into lateral and vertical components, these measurements will also guide an assessment of the potential impact of observed vertical velocity on the lateral wind velocity measured by the NSSL-MM. Since both wind velocity sensors are embedded in the vehicle-modified airstream, this intercomparison alone cannot be used to assess the impact of a vehicle-perturbed mean-state *lateral* flow on the observed lateral wind field. Thus, to complement the intercomparison, a suite of computational fluid dynamics (CFD) wind tunnel simulations of the vehicle have been conducted to approximate the modification of the airstream by the vehicle. The analysis focuses on the magnitudes of the vertical velocity and perturbation lateral velocity at the locations of the sensors in the simulations.

The wind tunnel simulations are computed using STAR-CCM+ (CD-adapco 2015), employing a finite volume solver for compressible, steady-state Navier–Stokes flow with the k–ε turbulence model (Mohammadi and Pironneau 1993). The model domain is 27.8 m long, 20.5 m wide, and 12 m tall. The upper and lower domain boundaries are free-slip.

The van is initialized using a computer-aided design (CAD) model for a 2000 Dodge Caravan. Although, a 2007 Dodge Caravan was used for the actual mobile mesonet, differences in the vehicle profiles were deemed to be negligible. The van is positioned within the domain approximately 4 van lengths from the front inlet, approximately three van lengths from the right inlet, one van length from the rear outlet, and one van length from the left outlet. There are 5.5 van heights from the roof to the top of the domain (Fig. 4). A polyhedral domain mesh (Fig. 4) is used. Cells are prescribed using an initially triangular mesh along the surface of the vehicle and domain boundaries that is then converted to polyhedrals within the STAR-CCM+ meshing algorithm.

In the interest of simplicity, the vehicle is modeled as a ''bluff body'' and the mobile mesonet rack is not included in the model. Although air should be allowed to enter the grill in the front of the vehicle, it is assumed that the air inside the engine compartment behind the grill is nearly stagnant, resulting in a negligible flux through the grill relative to the external flow deflected around the vehicle. The mobile mesonet rack (Fig. 2) has been designed to minimize its impact on the airstream at the wind monitor, and the forward-mounted Aeroprobe in the integrated system (Fig. 3) is largely immune to the (upstream) impact of the rack. The flow perturbation at the mobile mesonet wind monitor caused by the wing and Aeroprobe, which are mounted 35 cm ahead of and 55 cm below the monitor, respectively, is assumed to be negligible.

All simulations were executed for 300 iterations. This was sufficient to yield residuals for continuity, x, y, z momentum; energy; turbulent kinetic energy; and turbulent dissipation that were less than approximately 10^{-3}.

CFD experiments were designed to expose the sensitivity of the perturbation airstream at sensor level to 1) the vehicle-relative ambient along-axis airspeed v_0 (in practice this is a combination of vehicle speed and head wind) and 2) the ambient crosswind speed u_0. (The present study refers to the total velocity components in the along-axis, cross-axis, and vertical directions via the vector triplet $[v, u, w]$, respectively, with perturbation horizontal components defined as $v' = v - v_0$ and $u' = u - u_0$.) The ambient along-axis airspeed and crosswind speed were simulated using the modeled inlet speed through the domain boundary ahead of the vehicle and to the right of the vehicle, respectively. Along-axis

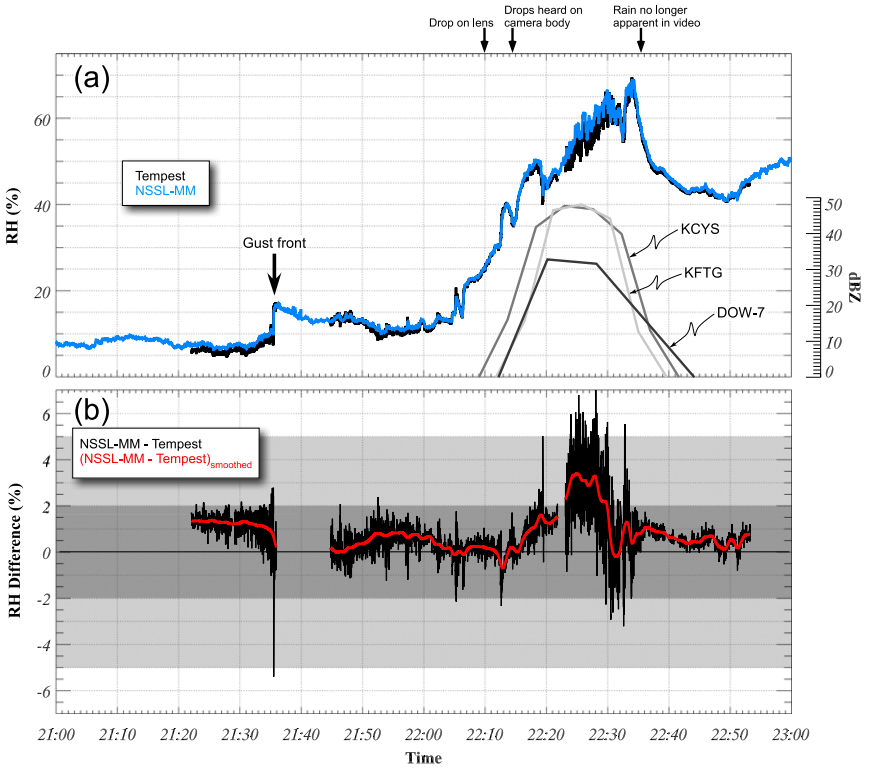

FIG. 5. (a) Tempest (black) and NSSL-MM (blue) time series of RH for the intercomparison drive on 21 Jun 2013. Gray curves are the radar reflectivity from the lowest scans of DOW7, KFTG, and KCYS at the location of the vehicle. (b) Absolute RH difference between the NSSL-MM and Tempest (black) and a spectrally smoothed profile (red). Light gray and dark gray regions are the accuracy ranges of the Tempest and NSSL-MM humidity sensors, respectively (refer to Table 1).

airspeed experiments involved 14 simulations with values between 10 and 36 m s^{-1}. Crosswind experiments involved 10 simulations with crosswind angles between 0° and 45° and a total inlet speed $(u_0^2 + v_0^2)^{1/2}$ of 30 m s^{-1}.

3. Results

a. Temperature/humidity sensors

On 21 June 2013, the integrated system was used to target a thunderstorm complex and associated gust front in northeast Colorado. The time series of relative humidity (RH), corrected to represent ambient RH using the approach of Richardson et al. (1998),[1] and temperature appear in Figs. 5 and 6, respectively. At 2135:29 UTC, the integrated system crossed a gust front that was almost exclusively manifested in the moisture field. As apparent in video recorded during the deployment and consistent with contemporaneous radar reflectivity measured by a Doppler on Wheels (DOW) mobile radar and the nearby KFTG (Denver, Colorado) and KCYS (Cheyenne, Wyoming) WSR-88D radars, the integrated system encountered occasionally heavy precipitation between ~2210 and ~2235 UTC.

Despite the exposure of the Tempest temperature and humidity sensors to the airstream, the time series of Tempest RH (black curve in Fig. 5a) and temperature (black curve in Fig. 6a) show no evidence of wet bulbing while encountering precipitation for nearly 25 min. In fact, during precipitation, the Tempest RH was actually slightly lower (Fig. 5b) and the temperature was slightly higher (Fig. 6b) than the NSSL-MM observations.

Overall, the time series structure (Figs. 5a and 6a) and instantaneous magnitudes (Figs. 5b and 6b) demonstrate the consistency between the NSSL-MM and Tempest temperature and humidity sensors. Closer examination of the instantaneous-difference time series (Figs. 5b and 6b) reveals that the NSSL-MM-corrected RH tends to be

[1] Applied to the NSSL-MM, the Richardson et al. (1998) correction uses the RH and slow temperature sensors combined within the HMP45C to calculate the dewpoint temperature and then it recalculates the RH using this dewpoint temperature and the fast temperature recorded by the YSI 405 thermistor.

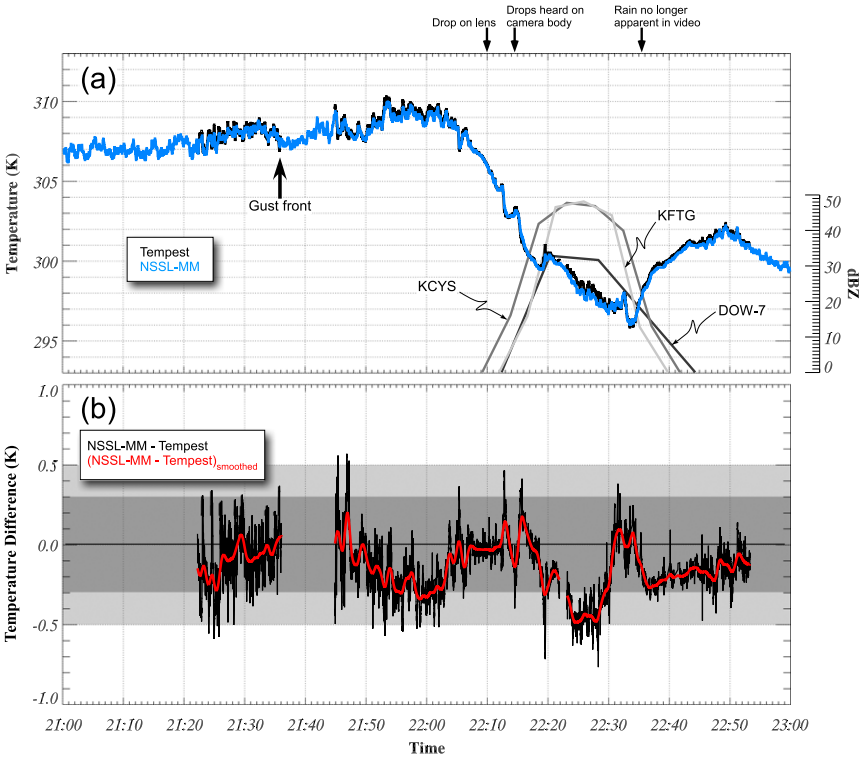

FIG. 6. (a) Tempest (black) and NSSL-MM (blue) time series of temperature for the intercomparison drive on 21 Jun 2013. Gray curves are the radar reflectivity from the lowest scans of DOW7, KFTG, and KCYS at the location of the vehicle. (b) Absolute temperature difference between the NSSL-MM and Tempest (black) and a spectrally smoothed profile (red). (Smoothing is performed using a Gaussian smoother with a 60-s width.) Light gray and dark gray regions are the accuracy ranges of the Tempest and NSSL-MM temperature sensors, respectively (refer to Table 1).

slightly higher (0.82%) than the Tempest RH over the 2100–2300 UTC 21 June 2013 analysis window and that the temperature tends to be slightly lower (−0.15 K). Overall, the differences between the NSSL-MM and Tempest temperature and humidity observations are generally within the accuracies of the sensors (gray shading in Figs. 5b and 6b). The largest differences in RH exist at the gust front crossing (~2135 UTC) and during heavy precipitation.

RH values for the NSSL-MM during the 25 min of precipitation averaged 1.3% higher than the RH measured by the Tempest. The mean differences increased to 2.7% for the period of heaviest precipitation between 2220 and 2230 UTC. It is hypothesized that this difference could be attributable to slight systematic differences in the airstream sampled by the NSSL-MM and Tempest temperature and humidity sensors. The base of the NSSL-MM U-tube (where the air is drawn across the NSSL-MM temperature and humidity sensors) was ~35 cm rearward and ~55 cm below the Tempest temperature/humidity sensor. The presence of rain splatter on the roadway could hypothetically produce a negative vertical gradient in RH in the near surface layer that is swept above the vehicle and across the sensors.

Differences associated with the gust front crossing at ~2135 UTC (Fig. 5b) are a consequence of differing time constants between the two sensors. The Tempest humidity sensor (RS92), which has a manufacturer-specified theoretical response time of <0.5 s, detected an RH increase of 6.5% across adjacent observations separated by 0.42 s (Fig. 7). The NSSL-MM humidity sensor (HMP45C) located within the U-tube required 17 s for a 90% response to this change (manufacturer specifications for the HMP45C list a 15-s period for a 90% response). Thus, the U-tube increased response time by ~13%. The origin of the occasional periods of missing (nonlogged) Tempest humidity observations is unknown.

b. *Simulated wind speeds above an NSSL-MM vehicle*

Wind tunnel simulations produce the expected distributions of perturbation along-axis flow v' (Fig. 8a) and

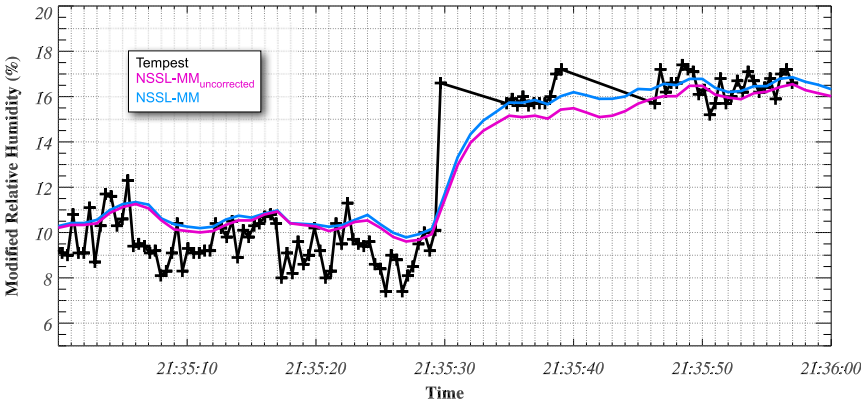

FIG. 7. Tempest (black) and NSSL-MM uncorrected (purple) and corrected (blue) time series of RH for the gust front crossing on 21 Jun 2013.

vertical velocity w (Fig. 8b) with rising motion upstream and near the leading edge of the vehicle and accelerated lateral flow ($v' > 0$) above the vehicle. Simulations conducted using a range of along-axis air speeds v_0 show a linear increase in v' at the locations of both the NSSL-MM wind monitor and the Tempest Aeroprobe (Fig. 9). For $v_0 =$ 30–35 m s^{-1} (i.e., typical highway speeds) simulated v' at the NSSL-MM wind monitor are 1.2–1.5 m s^{-1} For all considered values of v_0, the simulated winds (v) were ~4% faster than the expected winds (v_0). Simulations also reveal that v' at the location of the NSSL-MM wind monitor exceeds the v' at the lower- and forward-mounted Tempest Aeroprobe by as much as 0.83 m s^{-1} and that the difference scales directly with the along-axis airspeed. However, the ratio of the *total* along-axis flow at the location of the NSSL-MM wind monitor to the total along-axis flow at the location of the Tempest Aeroprobe is virtually independent of v_0. The simulated total along-axis flow is 2.2% stronger at the location of the NSSL-MM wind monitor than the flow at the Aeroprobe location.

The simulated vertical velocity exceeds the perturbation along-axis flow at the locations of both the NSSL-MM wind monitor and the Aeroprobe. For $v_0 =$ 30 m s^{-1}, the simulated w has a value of 1.31 m s^{-1} at the NSSL-MM wind monitor location and 2.04 m s^{-1} at the Tempest Aeroprobe location. As with v', w scales linearly with the along-axis wind speed (Fig. 10). Vertical velocities in all of the along-axis airspeed experiments are larger at the location of the Tempest Aeroprobe. The relative difference between the vertical velocity values is largely independent of v_0: simulated w at the location of the NSSL-MM wind monitor is ~64% of the w at the location of the Tempest Aeroprobe.

Crosswind experiments reveal somewhat more complex relationships between the perturbed flow and the crosswind angle than the linear relationships exhibited in the along-axis airspeed results. In general, the perturbation lateral airspeed, $|\mathbf{V}|' = (u^2 + v^2)^{1/2} - (u_0^2 + v_0^2)^{1/2}$, is found to increase with increasing crosswind angle for angles exceeding 5° (Fig. 11). At crosswind angles of ~45°, the differences from the expected wind speed exceed 9% at the location of the NSSL-MM wind monitor. In contrast to the perturbation lateral airspeed, vertical velocity is found to change very little as a function of crosswind angle (Fig. 12).

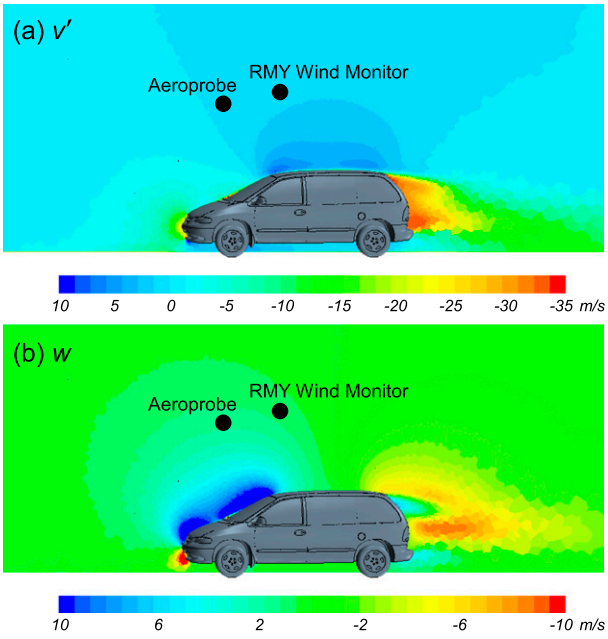

FIG. 8. Simulated distributions of (a) v' and (b) w for an inlet speed of 30 m s^{-1}.

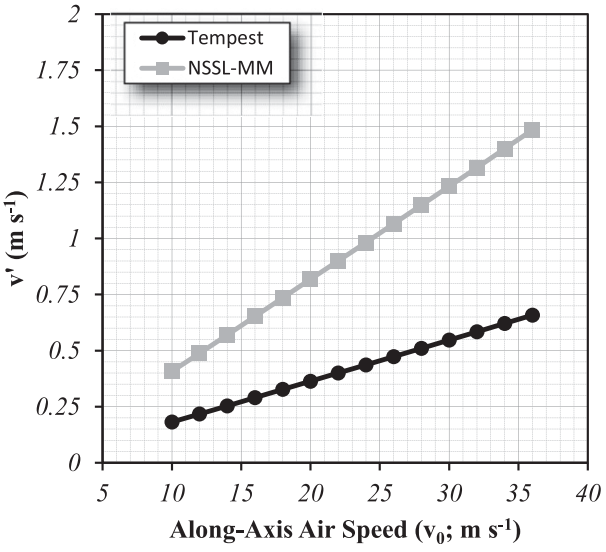

FIG. 9. Simulated relationship between v_0 and v'.

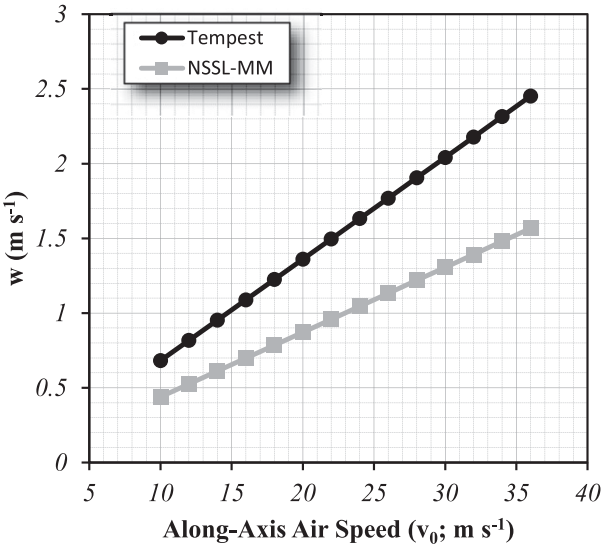

FIG. 10. Simulated relationship between v_0 and w.

c. *Comparison of simulated and observed wind speeds above an NSSL-MM vehicle*

In an effort to gauge the reliability of the simulations, a comparison is made to the body-relative components of the flow observed during AVIATE. For the AVIATE observations, v_0 and v' are unknown because the head wind is unknown. However, the veracity of the simulations can still be assessed by comparing the difference between the airspeeds at the locations of the NSSL-MM wind monitor and the Tempest Aeroprobe within the simulation to the difference that was observed.

Postprocessing of the AVIATE data recorded by the Aeroprobe revealed a slight misalignment of the sensor that impacted the accurate decomposition of the flow. The cross-axis misalignment was estimated using the body-relative wind direction. Because the intercomparison was largely conducted using data collected while the vehicle was traveling at highway speeds, the body-relative wind direction should exhibit a clustering near 0°. This behavior is manifested in the NSSL-MM data for the 2 h of data collected on 20 June during AVIATE (Fig. 13a). However, the uncorrected Aeroprobe body-relative wind direction for the same period exhibits a bias toward negative values (Fig. 13b) that is consistent with a probe that is laterally misaligned by ~0.37°. The Aeroprobe data were corrected by adjusting the body-relative wind direction and recalculating u and v assuming that the wind speed was unchanged.

A possible vertical misalignment was also considered. The Tempest Aeroprobe w is found to be considerably larger than the simulated vertical velocity (Fig. 14). For a v ~30 m s^{-1}, the median observed w is 5.44 m s^{-1}, whereas the simulated w is 2.06 m s^{-1}. The magnitude of the bias is unlikely to be solely a consequence of simulation errors and is likely partly caused by a vertical misalignment of the Aeroprobe: the probe was likely tilted up a small amount (as corroborated from visual inspection of Fig. 3b, which suggests a small clockwise rotation of the mounted wing relative to the instrument rack), thereby artificially increasing the observed w and artificially decreasing v. Adjusting the observed w for a vertical misalignment of 6.3° at v ~30 m s^{-1} would produce a median w equivalent to the simulated w (corrected w values assuming vertical misalignments of 3°

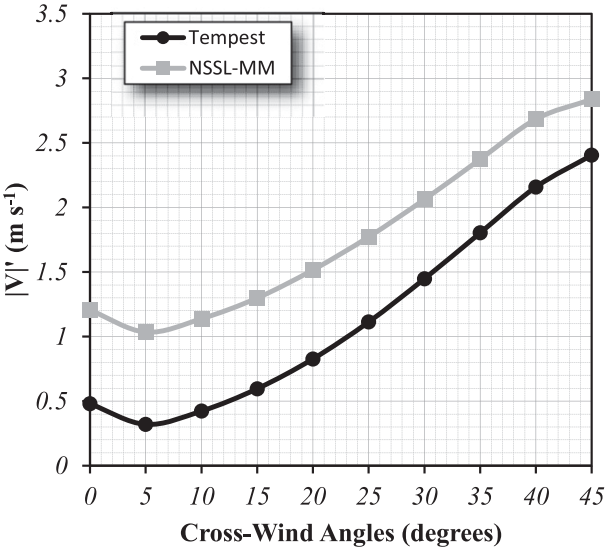

FIG. 11. Simulated relationship between crosswind angle and $|\mathbf{V}|'$.

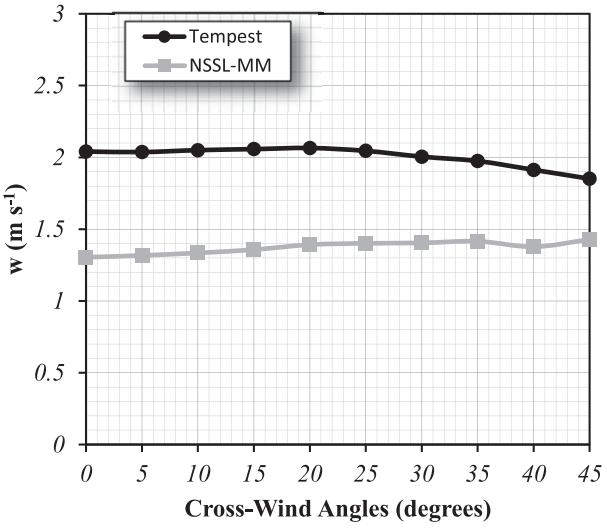

FIG. 12. Simulated relationship between crosswind angle and w.

and 6.3° are plotted in Fig. 14). The precise value of inferred misalignment is unknown but a value of 6.3° will serve as a useful point of reference for the following analysis.

As noted above, since the observed u_0 and v_0 are unknown, the simulated results will be assessed by comparing the difference between the flow at the locations of the NSSL-MM wind monitor and the Tempest Aeroprobe within the simulation to the difference that was observed. The simulated (observed) difference in the along-axis flow will be denoted Δv_{sim} (Δv_{obs}), where $\Delta v = v_N - v_T$, and v_N (v_T) is the along-axis flow for the NSSL-MM wind monitor (Tempest Aeroprobe). The along-axis airspeed numerical experiments will be used for comparing Δv_{sim} to Δv_{obs}, while the crosswind experiments will be used for comparing Δu_{sim} to Δu_{obs}.

Both Δv_{obs} (calculated from data collected on 20 June 2013) and Δv_{sim} reflect generally stronger v at the NSSL-MM wind monitor than the Tempest Aeroprobe (Fig. 15). Based on a least squares regression line calculated assuming a zero intercept (green line in Fig. 15), the relative differences ($\Delta v/v_N$) are 1.6%, 2.1%, and 2.9% for assumed vertical misalignments of 6.3°, 3°, and 0°, respectively (data for an assumed misalignment of 6.3° are illustrated in Fig. 15). These values are all comparable to the simulated relative difference of 2.2% and indicate close correspondence between the simulated results and observations. However, it does not serve to verify the accuracy of the absolute magnitude of the simulated v.

Comparisons of Δu_{sim} (using the crosswind experiments) to Δu_{obs} reveal a poorer agreement between the simulated and observed Δu. To facilitate a comparison to the simulated data (for which the inlet speed was set to 30 m s^{-1}), only observations in the interval $v \in [29, 31\ \text{m s}^{-1}]$ are considered for the following analysis. Furthermore, no vertical misalignment correction is performed as it was found to have no significant impact on u. Using the least squares regression to the observed data (green line in Fig. 16), the observed relative difference ($\Delta u/u_N$) is 17.5%, whereas the simulated relative difference across the range of observed u (approximately $\pm 7\ \text{m s}^{-1}$ corresponding to approximately ±13°) is 1.5% (Fig. 16). Moreover, the median observed Δu for a body-relative direction of ~5° is 0.53 m s^{-1}, whereas the simulated Δu for a 5° crosswind angle is nearly an order of magnitude smaller (0.058 m s^{-1}). This comparison challenges the reliability of the crosswind

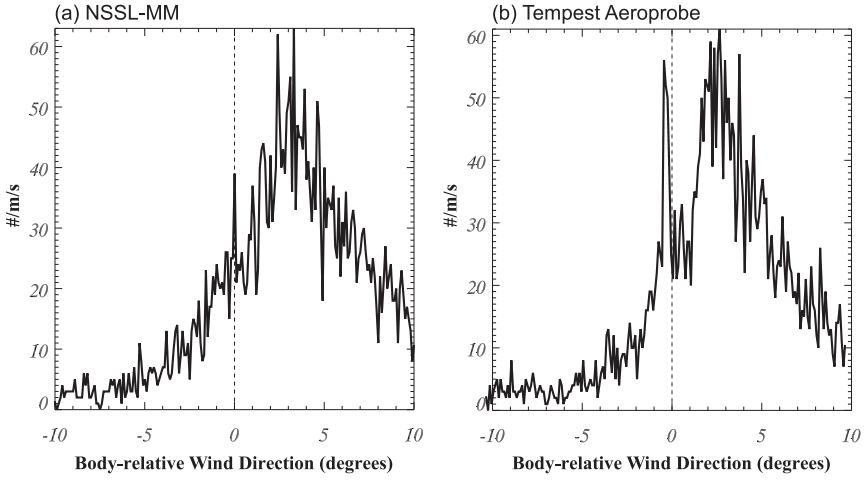

FIG. 13. Histograms of u from 20 Jun 2013 for the (a) NSSL-MM and (b) Tempest Aeroprobe (uncorrected for lateral misalignment).

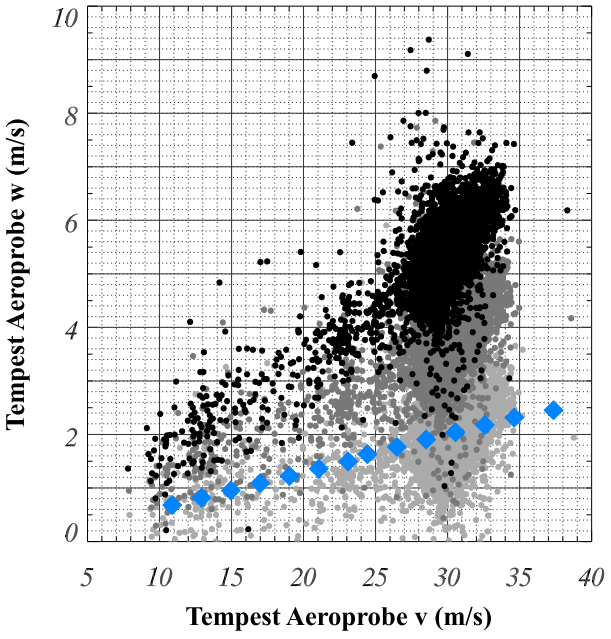

FIG. 14. Uncorrected w (black circles) plotted as a function of v from the 20 Jun 2013 intercomparison for the Tempest Aeroprobe. Dark (light) gray circles are the corrected w assuming a vertical misalignment of 3° (6.3°). Blue diamonds represent the values simulated in the along-axis speed experiments.

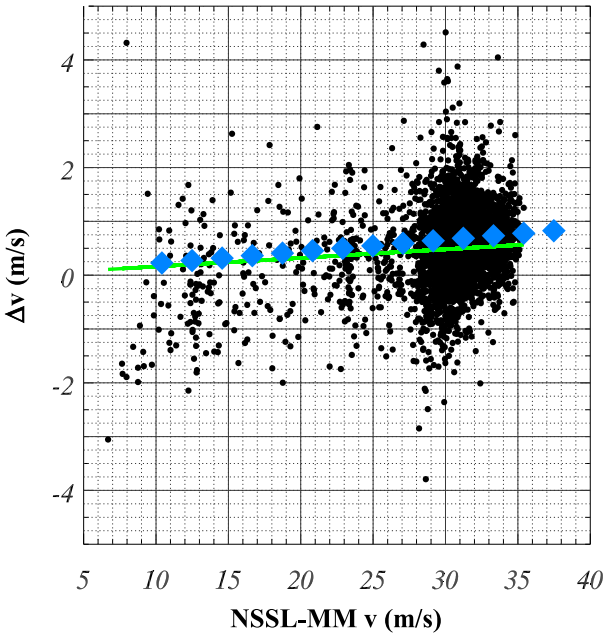

FIG. 15. Observed (black circles) and simulated (blue diamonds) $\Delta v = v_N v_T$ as a function of the NSSL-MM wind monitor v. Observations are from the 20 Jun 2013 intercomparison and assume a vertical misalignment of 6.3°. A least squares regression fit to the observed data is illustrated with a green line.

simulations. In contrast to conditions for which the flow is predominantly along the vehicle axis, a crosswind should be expected to interact with the quasi-vertical side of the MM vehicle to produce significant dynamic pressure and associated accelerations along with appreciable turbulence that is likely to yield discrepancies with the steady-state solution of the simulated flow field. It is therefore unsurprising that the simulations tend to disagree with observations for simulated crosswind conditions.

Discrepancies between the simulations and the observations could also stem from the response of the NSSL-MM wind monitor to an airstream with a significant vertical component. For a constant wind speed in the y–z (along-axis and vertical axis) plane ($\mathbf{V}_{y-z}$), v should theoretically scale with the cosine of the angle α, the angle of the y–z velocity vector relative to y. However, vertical velocity will reduce the rotation speed of horizontally oriented propeller anemometers (Holmes et al. 1964; Drinkrow 1972). This noncosine response is characterized by a peak absolute reduction in rotation speed for $\alpha = \pi/4$ and peak relative reduction for $\alpha = \pi/2$ (Drinkrow 1972). Through adaptation of the results of Drinkrow, the theoretical reduction in v due to the noncosine response can be related to w for a given lateral airspeed (Fig. 17). For a lateral airspeed of $30\,\mathrm{m\,s^{-1}}$, the noncosine reduction in v is found to be negligible across the range of vertical velocities that were observed and simulated. Specifically, for $w = 1.3\,\mathrm{m\,s^{-1}}$ (i.e., the simulated vertical velocity at the location of the NSSL-MM wind monitor) the relative reduction is only 0.11%. Interestingly, the reduction scales inversely with

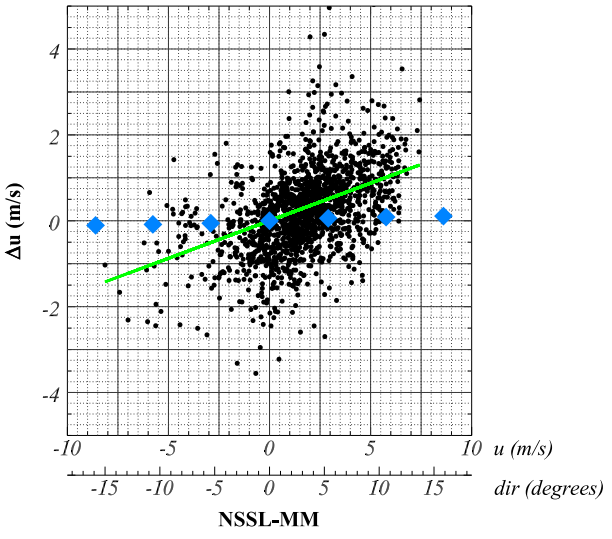

FIG. 16. Observed (black circles) and simulated (blue diamonds) $\Delta u = u_N - u_T$ as a function of the NSSL-MM wind monitor u. Observations are from the 20 Jun 2013 intercomparison. A least squares regression fit to the observed data is illustrated with a green line.

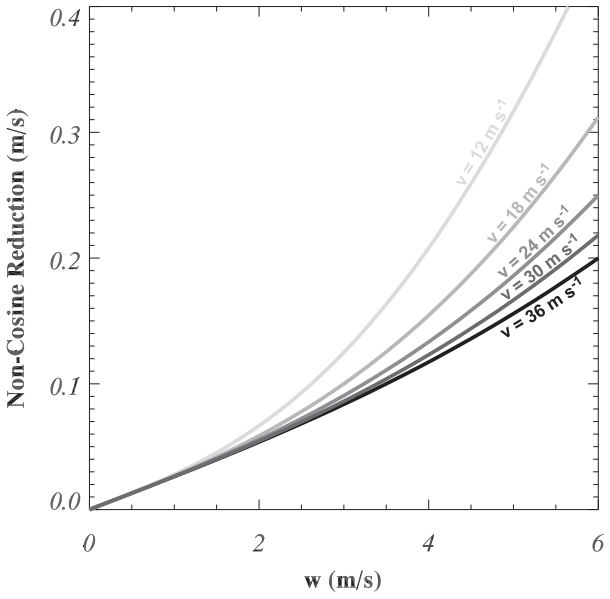

FIG. 17. Theoretical reduction in the observed horizontal wind speed due to the presence of a vertical component to the velocity.

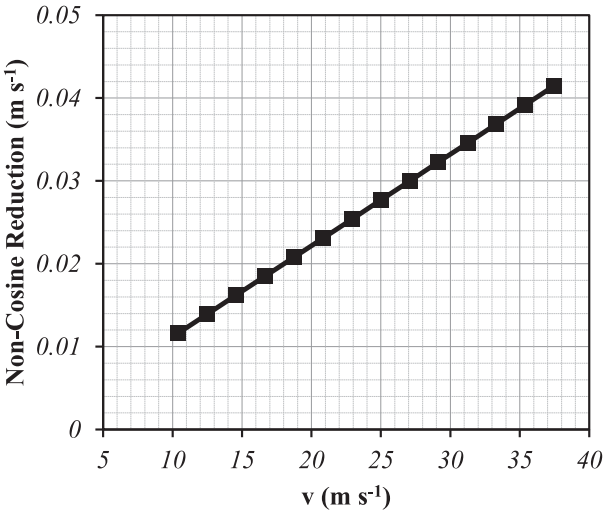

FIG. 18. Theoretical noncosine reduction in the horizontal wind speed based on simulated airflow.

the lateral airspeed for a given w (Fig. 17). However, this relationship neglects the dependence of w on v within the airstream over a vehicle (Fig. 10). The noncosine reduction in v calculated using the simulated v and w (Fig. 18) reveals that the noncosine reduction scales directly with v and is negligible across the range of v considered.

4. Summary

The Airdata Verification and Integrated Airborne Tempest Experiment (AVIATE) was conducted in June 2013 with the aim to compare the meteorological sensors aboard the Tempest UAS and the NSSL mobile mesonet (MM). The increasing popularity of UAS as platforms for conducting atmospheric science means that the results of sensor intercomparisons and the methodologies for conducting them need to be documented. Moreover, the dearth of studies evaluating the performance of the meteorological sensors included in the MM further justifies the intercomparison documented herein. Contemporaneous evaluation of sensor performance was facilitated by mounting the Tempest wing with attached sensors to the NSSL-MM instrument rack such that the Tempest and NSSL-MM sensors could collect observations within a nearly identical airstream. This intercomparison was complemented by CFD wind tunnel simulations designed to evaluate the impact of the NSSL-MM vehicle on the observed wind velocity.

Experiments were designed to address three potential performance issues: exposure of the Tempest temperature/moisture sensor makes it susceptible to wetting in precipitation and erroneous wet bulbing; the U-tube housing for the temperature/moisture sensors of the NSSL-MM reduces the sensor response; and the NSSL-MM vehicle will significantly modify the wind field above the vehicle, which could have a significant impact on the observed wind velocity. Principal findings from the intercomparison are as follows:

- The temperature and relative humidity (RH) data collected by the Tempest and the NSSL-MM correspond very well: the NSSL-MM-corrected RH tends to be slightly higher (0.82%) than the Tempest RH and the temperature tends to be slightly lower (−0.15 K). These differences are within the accuracies of the sensors.
- Observed differences in RH were found to increase to 2.7% in the presence of heavy precipitation. It is hypothesized that the presence of rain splatter on the roadway might produce a negative vertical gradient in RH in the near-surface layer that is swept above the vehicle and across the sensors, leading to the NSSL-MM sensors (mounted lower on the rack) to record higher RH.
- Despite the exposure of the Tempest temperature and humidity sensors to the airstream, there was no evidence of wet bulbing while encountering heavy precipitation.
- CFD wind tunnel simulations conducted using a range of along-axis airspeeds (v_0) show a linear increase in the perturbation along-axis flow (v') at the locations of both the NSSL-MM wind monitor and the Tempest Aeroprobe. For all values of v_0 considered, the simulated

winds (v) at the location of the NSSL-MM wind monitor were ~4% larger than the expected winds (v_0).

- Simulated vertical velocity at the location of the NSSL-MM wind monitor exceeds 1 m s^{-1} for v_0 values typical of a vehicle moving at highway speeds and scales linearly with v_0.
- Crosswind numerical experiments reveal that the perturbation lateral airspeed $|\mathbf{V}|' = (u^2 + v^2)^{1/2} - (u_0^2 + v_0^2)^{1/2}$ increases with the increasing crosswind angle and exceeds 9% for crosswind angles of ~45°.
- To gauge the reliability of the simulations, the difference between the airspeeds at the locations of the NSSL-MM wind monitor and the Tempest Aeroprobe—$\Delta v = v_N - v_T$, where v_N (v_T) is the along-axis flow for the NSSL-MM wind monitor (Tempest Aeroprobe)—are compared between the simulations and the observations. Both Δv_{obs} and Δv_{sim} are generally positive, reflecting stronger v at the NSSL-MM wind monitor than the Tempest Aeroprobe. Relative differences ($\Delta v/v_N$), even allowing for some uncertainty in the degree of Tempest Aeroprobe vertical misalignment, indicate close correspondence between the simulated results and observations. However, the absolute magnitude of the simulated v is difficult to assess without knowing the actual observed head wind.
- Comparisons of Δu_{sim} (using the crosswind experiments) to Δu_{obs} reveal a poorer agreement between the simulated and observed Δu that challenges the reliability of the crosswind simulations. It is hypothesized that the interaction of a crosswind with the side of the vehicle makes the steady-state assumption of the CFD simulations more prone to error.
- The noncosine reduction in v that would theoretically result from the impact of vertical velocity on the laterally mounted wind monitor was found to be negligible across the range of v considered.

Although not addressed in this article, the intercomparison also revealed potential errors produced when thermodynamic quantities, such as equivalent potential temperature, are derived using temperature and moisture measured by sensors with dramatically different response times (Houston et al. 2014). Future work will aim to further examine this source of error. Future work could also extend the results of the CFD simulations by considering the impact of the mesonet rack on the flow field.

Acknowledgments. The authors are grateful to the two anonymous reviewers, whose comments and corrections greatly improved the quality of this article. Authors ALH, RJL, TWN, and BA were funded by Air Force Office of Scientific Research Grant FA9550-12-1-0412 to conduct this work. The NSSL-loaned Aeroprobe five-port probe and funding to install it on the Tempest was provided for AVIATE by the NSSL under a Director's Discretionary Research Fund (DDRF) grant to coauthor CLZ. The NSSL DDRF grant also provided funding for the NSSL Field Observing Facilities Support group to mount the Tempest on the NSSL MM and travel support for the NSSL coauthors to participate in AVIATE. The Center for Severe Weather Research is gratefully acknowledged for providing Doppler on Wheels mobile radar coverage during AVIATE. The Colorado State University CHILL radar is also acknowledged for providing additional radar support. The authors also acknowledge the field deployment support provided by the Research and Engineering Center for Unmanned Vehicles pilot/flight engineer James Mack.

REFERENCES

Aeroprobe Corp., 2012: On-the-Fly! Air Data System. User's Manual, Revision F, 16 pp.

CD-adapco, 2015: The world's most comprehensive engineering simulation inside a single integrated package. Accessed 28 August 2015, Computational Dynamics–Analysis and Design Application Company. [Available online at http://www.cd-adapco.com/products/star-ccm%C2%AE.]

Douglas, M. W., 2008: Progress towards development of the glidersonde: A recoverable radiosonde system. *WMO Tech. Conf. on Meteorological and Environmental Instruments and Methods of Observation (TECO-2008)*, St. Petersburg, Russia, World Meteorological Organization, P1(6). [Available online at https://www.wmo.int/pages/prog/www/IMOP/publications/IOM-96_TECO-2008/P1%2806%29_Douglas_USA.pdf.]

Drinkrow, R., 1972: A solution to the paired Gill-anemometer response function. *J. Appl. Meteor.*, **11**, 76–80, doi:10.1175/1520-0450(1972)011<0076:ASTTPG>2.0.CO;2.

Elston, J. S., J. Roadman, M. Stachura, B. Argrow, A. L. Houston, and E. W. Frew, 2011: The Tempest Unmanned Aircraft System for in situ observations of tornadic supercells: Design and VORTEX2 flight results. *J. Field Rob.*, **28**, 461–483, doi:10.1002/rob.20394.

——, B. Argrow, M. Stachura, D. Weibel, D. Lawrence, and D. Pope, 2015: Overview of small fixed-wing unmanned aircraft for meteorological sampling. *J. Atmos. Oceanic Technol.*, **32**, 97–115, doi:10.1175/JTECH-D-13-00236.1.

Frew, E. W., J. Elston, B. Argrow, A. L. Houston, and E. N. Rasmussen, 2012: Sampling severe local storms and related phenomena: Using unmanned aircraft systems. *IEEE Rob. Autom. Mag.*, **19**, 85–95, doi:10.1109/MRA.2012.2184193.

Holland, G. J., and Coauthors, 2001: The Aerosonde robotic aircraft: A new paradigm for environmental observations. *Bull. Amer. Meteor. Soc.*, **82**, 889–901, doi:10.1175/1520-0477(2001)082<0889:TARAAN>2.3.CO;2.

Holmes, R. M., G. C. Gill, and H. W. Carson, 1964: A propellor-type vertical anemometer. *J. Appl. Meteor.*, **3**, 802–804, doi:10.1175/1520-0450(1964)003<0802:APTVA>2.0.CO;2.

Houston, A. L., B. Argrow, J. Elston, J. Lahowetz, E. W. Frew, and P. C. Kennedy, 2012: The Collaborative Colorado–Nebraska Unmanned Aircraft System Experiment. *Bull. Amer. Meteor. Soc.*, **93**, 39–54, doi:10.1175/2011BAMS3073.1.

——, R. J. Laurence III, T. Nichols, S. Waugh, B. Argrow, and C. Ziegler, 2014: Errors in mobile mesonet observations of equivalent potential temperature and wind velocity: Results from the Airdata Verificaton and Integrated Airborne Tempest Experiment (AVIATE). *27th Conf. on Severe Local Storms*, Madison, WI, Amer. Meteor. Soc., 137. [Available online at https://ams.confex.com/ams/27SLS/webprogram/Paper254893.html.]

Lang, T. J., and Coauthors, 2004: The Severe Thunderstorm Electrification and Precipitation Study. *Bull. Amer. Meteor. Soc.*, **85**, 1107–1125, doi:10.1175/BAMS-85-8-1107.

Markowski, P. M., 2002: Mobile mesonet observations on 3 May 1999. *Wea. Forecasting*, **17**, 430–444, doi:10.1175/1520-0434(2002)017<0430:MMOOM>2.0.CO;2.

Mohammadi, B., and O. Pironneau, 1993: *Analysis of the K-Epsilon Turbulence Model.* Masson, 194 pp.

Rasmussen, E. N., J. M. Straka, R. P. Davies-Jones, C. A. Doswell III, F. H. Carr, M. D. Eilts, and D. R. MacGorman, 1994: Verification of the Origins of Rotation in Tornadoes Experiment: VORTEX. *Bull. Amer. Meteor. Soc.*, **75**, 995–1006, doi:10.1175/1520-0477(1994)075<0995:VOTOOR>2.0.CO;2.

Richardson, S. J., S. E. Frederickson, F. V. Brock, and J. A. Brotzge, 1998: Combination temperature and relative humidity probes: Avoiding large air temperature errors and associated relative humidity errors. Preprints, *10th Symp. on Meteorological Observations and Instrumentation*, Phoenix, AZ, Amer. Meteor. Soc., 278–283.

Skinner, P. S., C. C. Weiss, A. E. Reinhart, W. S. Gunter, J. L. Schroeder, and J. Guynes, 2010: TTUKa mobile Doppler radar observations of near-surface circulations in VORTEX2. *25th Conf. on Severe Local Storms*, Denver, CO, Amer. Meteor. Soc., 15.3. [Available online at https://ams.confex.com/ams/25SLS/techprogram/paper_176236.htm.]

Straka, J. M., E. N. Rasmussen, and S. E. Fredrickson, 1996: A mobile mesonet for finescale meteorological observations. *J. Atmos. Oceanic Technol.*, **13**, 921–936, doi:10.1175/1520-0426(1996)013<0921:AMMFFM>2.0.CO;2.

Waugh, S., and S. E. Frederickson, 2010: An improved aspirated temperature system for mobile meteorological observations, especially in severe weather. *25th Conf. on Severe Local Storms*, Denver, CO, Amer. Meteor. Soc., P5.2. [Available online at https://ams.confex.com/ams/25SLS/techprogram/paper_176205.htm.]

Weckwerth, T. M., and Coauthors, 2004: An overview of the International H_2O Project (IHOP_2002) and some preliminary highlights. *Bull. Amer. Math. Soc.*, **85**, 253–277, doi:10.1175/BAMS-85-2-253.

Wurman, J., D. Dowell, Y. Richardson, P. Markowski, E. Rasmussen, D. Burgess, L. Wicker, and H. B. Bluestein, 2012: The Second Verification of the Origins of Rotation in Tornadoes Experiment: VORTEX2. *Bull. Amer. Meteor. Soc.*, **93**, 1147–1170, doi:10.1175/BAMS-D-11-00010.1.

Ziegler, C. L., E. N. Rasmussen, M. S. Buban, Y. P. Richardson, L. J. Miller, and R. M. Rabin, 2007: The ''triple point'' on 24 May 2002 during IHOP. Part II: Ground-radar and in situ boundary layer analysis of cumulus development and convection initiation. *Mon. Wea. Rev.*, **135**, 2443–2472, doi:10.1175/MWR3411.1.